Composites: Part A 166 (2023) 107379

Contents lists available at ScienceDirect

Composites Part A

journal homepage: www.elsevier.com/locate/compositesa

Graphene/polyurethane nanocomposite coatings – Enhancing the mechanical properties and environmental resistance of natural fibers for masonry retrofitting

Ali Abbass [a,*], Maria C. Paiva [b,*], Daniel V. Oliveira [a], Paulo B. Lourenço [a], Raul Fangueiro [c]

[a] Department of Civil Engineering, University of Minho, ISISE, 4800-058 Guimarães, Portugal
[b] Department of Polymer Engineering, University of Minho, IPC, 4800-058 Guimarães, Portugal
[c] Department of Textile Engineering, University of Minho, 2C2T, 4800-058 Guimarães, Portugal

ARTICLE INFO

Keywords:
A-Natural fibers
A-Graphene
D-Mechanical testing
E-Surface treatments

ABSTRACT

Natural fibers form economic and environmentally friendly substitutes for synthetic fibers in civil engineering composites. However, natural fibers present flaws, irregular morphology and reduced durability in alkaline media. The present work reports the application of a new nanocomposite-based coating for flax and hemp fibers that enhances their mechanical properties and environmental resistance. The nanocomposite coating is based on graphene nanoplatelets (GNPs) and a waterborne polyurethane (WPU). Nanocomposites were prepared with pristine and surface modified GNPs, the latter obtained by polydopamine self-polymerization, tailoring the surface chemistry for strong interfaces with polyurethane. The coated fibers demonstrate enhanced tensile properties and low water absorption. Hemp yarns present 120% and 163% increases in tensile strength and elastic modulus, respectively, compared to the as-received yarns. The yarn properties achieved are adequate for their application as reinforcement of brittle and hydrophilic matrices such as lime, thus setting a new milestone in natural fiber composites manufacturing.

1. Introduction

The historical masonry is characterized by low mechanical performance and brittle behavior compared to modern materials like reinforced concrete or steel constructions [1]. Such specific structures are highly susceptible to natural and manmade hazards, an issue that entails the need for structural interventions to mitigate the consequent damages. Amongst the different techniques employed for strengthening and repairing of masonry-built heritage, textile reinforced mortar (TRM) systems have delivered a compatible structural solution that allows masonry breathability [2 3]. The reinforcements utilized in TRM system are usually prepared from strong synthetic fibers, such as glass, carbon and steel. Nonetheless, natural fibers have shown potential as an alternative to synthetic fibers for composite materials manufacturing, specifically for applications where reinforcements with low-to-medium mechanical properties favor the mechanical compatibility criteria [4 5]. In this context natural fibers constitute an economic, environmentally-friendly and mechanically suitable candidate for manufacturing natural fiber textile reinforced mortars (NTRM).

The research on the application of NTRM has started recently, however with limitations concerning structural behavior and durability [6]. Hence, the advantages of natural fibers come along with the challenges associated to composite preparation using cement or lime matrices. The natural fiber has a lignocellulosic composition that results in fiber hydrophilicity, facilitating its degradation upon the absorption of highly alkaline pore water present in the hydrophilic mortars, rich in deleterious hydration salts [7]. Such drawbacks may be overcome by means of a structural coating that endows the NTRM with the required performance, enhanced durability and ageing resistance. Moreover, it is critical that the coating meets environmental requirements to match the purpose of using natural fibers.

In the literature, several commercial coating protocols were proposed based on different types of epoxy or resins. Some of those coatings do not address the environmental aspects and improvement of the natural fiber's physical and mechanical properties. For instance, polyester-based coatings were widely used as sealer agents of natural fibers. Mercedes [5 8] employed polyester and epoxy coatings on different natural fibers and observed improvement of the yarn mechanical

* Corresponding authors.
E-mail addresses: id8215@alunos.uminho.pt (A. Abbass), mcpaiva@dep.uminho.pt (M.C. Paiva).

https://doi.org/10.1016/j.compositesa.2022.107379
Received 1 August 2022; Received in revised form 9 December 2022; Accepted 10 December 2022
Available online 13 December 2022

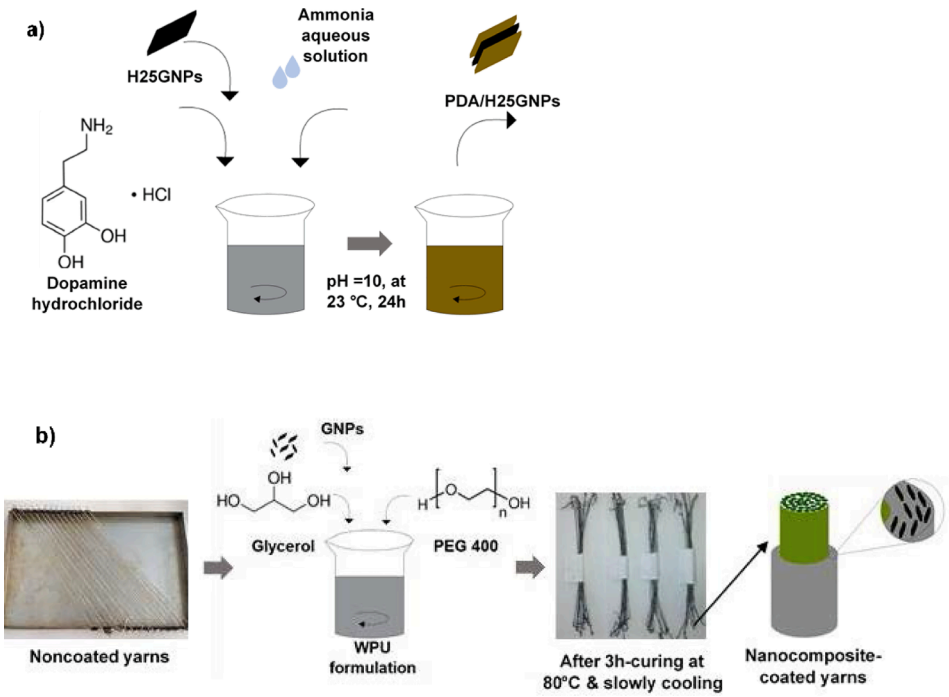

Fig. 1. Full coating procedure: a) PDA-functionalization of H25GNPs, b) coating/film casting protocol.

properties for both polymer coatings, epoxy-coated yarns providing higher composite performance [8]. Veigas et al. [9] tested different polymer coatings for sisal fibers, including polyesters resins, detecting the formation of voids in the matrix adjacent to the coated fibers, which could be associated to absorption of pore water from the cementitious matrix by the coating itself. The use of water-based styrene butadiene rubber (SBR) coating is considered a green protocol and was studied by Ferreira et al. [10] resulting in minor improvement in water absorption resistance of sisal fibers (fiberś water saturation was observed at 150 wt % gain if compared to 200 % in the noncoated sisal). Ferrara et al [11] detected an increase of the elastic modulus yet a drop in tensile strength of the flax yarns upon coating with carboxylated styrene butadiene rubber (XSBR). The composites prepared with the latter coated flax delivered an improved composite behavior as compared to the non-coated flax. Similarly, the bast fibers (i.e., Jute) studied by Ferreira et al. [12] experienced a reduction in the mechanical properties after using XSBR. Based on the literature, there is a fundamental need to engineer a coating formulation that assist bast-based natural fiber yarns to overcome their poor durability, low elastic modulus and weak interfacial bonding, employing environmentally friendly protocols.

In this paper, the authors present a structural coating that matches the environmental and mechanical criteria using waterborne polyurethane (WPU). WPU is an environmentally friendly polyurethane water-based suspension that is temperature-cured into films with only water as a curing by-product [13]. WPU is widely used in composites, adhesives, paints and coating engineering for large scale applications [14 15 16]. WPU films may have their expected lifespan reduced due to microcracking, which affects both the mechanical and physical properties of the polymer [17]. Therefore, in this work the improvement of WPU structural and physical properties was carried out through reinforcing the polymer with graphene nanoplatelets (GNPs) to produce nanocomposites with adequate mechanical behavior and improved physical properties. Furthermore, aiming at inducing chemical reactivity between the WPU and the GNPs, the authors propose the chemical functionalization of GNPs by means of the bio-based Mussel-inspired chemistry through the self-polymerization of dopamine into polydopamine (PDA) and its adsorption onto the GNPs. The self-polymerized PDA is a versatile coating that can adhere to most organic and inorganic surfaces as it is rich in highly reactive catechol and amine functional groups [18 19]. Such surface modification technique can improve the interfacial reactivity between the polymer and the nanoparticles as well as the dispersion quality of GNPs in water-based polymers. To the best of the author's knowledge, the proposed dip-dry/sprayed nanocomposite coatings were not yet introduced to civil engineering applications in general, and in particular to the strengthening of built heritage. The coated natural fibers delivered in this study may be considered as composite natural fibers with potential to become a milestone in NTRM manufacturing and pave the way for new technologies in the civil engineering sector.

2. Experimental campaign

2.1. Materials and methods

All materials, reagents, synthesis and coating casting, are described in the supplementary materials.

2.1.1. Functionalization of graphite nanoplatelets

The functionalization procedure is presented in Fig. 1a). Detailed description is provided in supplementary materials.

2.1.2. Preparation of polyurethane/ nonfunctionalized GNPs nanocomposites

PEG (dispersing agent) and GL (polymer plasticizer) (2 ml of each) were dissolved in 100 ml of WPU by magnetic stirring using IKA RCT basic Magnetic Hot Plate Stirrer at room temperature for 30 min. Then the GNPs were added to the mixture and ultrasonicated for 30 min, keeping the mixture in a cold-water bath. Three GNPs suspensions were prepared with reinforcement ratios of 0.5 %, 1 % and 2 % w:v of GNPs: PU. WPU/GNPs nanocomposites without PEG and GL were prepared following the same protocol and at the same reinforcement ratios. Films were cast and then cured in a convection oven at 80 °C for three hours and let cool slowly overnight, see Fig. 1b).

Table 1
Designation of the nanocomposites-based coating.

Nanocomposite ID	Percentage of nanoplateletes (wt. % relative to PU)	Dispersant and plasticizer
WPU/H25GNPs/0.5 %	0.5 %	With PEG/GL
WPU/PDA/H25GNPs/ 0.5 %	(PDA/H25GNPs) 0.5 %	With PEG/GL
WPU/H25GNPs/1%	1 %	With PEG/GL
WPU/H25GNPs/2%	2 %	With PEG/GL
WPU/H25GNPs/0.5 %–no PEG/GL	0.5 %	Without PEG/GL
WPU/H25GNPs/1%–no PEG/GL	1 %	Without PEG/GL
WPU/H25GNPs/2%–no PEG/GL	2 %	Without PEG/GL
WPU/CGNPs/0.5 %	0.5 %	With PEG/GL

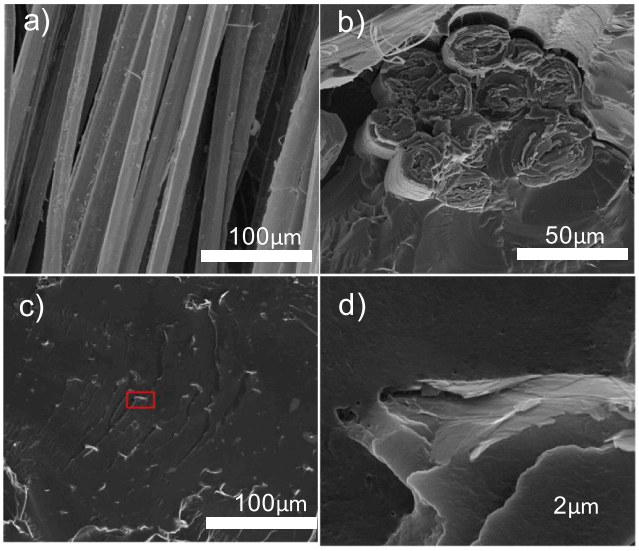

Fig. 2. SEM micrographs: a) surface of the pristine hemp yarns, b) cross-section of hemp-WPU/H25GNPs/0.5%, c) H25GNPs distribution in WPU/H25GNPs/ 0.5%, d) H25GNPs-to-WPU interface in WPU/H25GNPs/0.5%,

2.2. Characterization and testing

2.2.1. Tensile testing

Direct tensile tests were carried out on hemp and flax yarns before and after coating, testing 10 samples for each coating composition, see Table 1. The samples were kept under laboratory conditions for at least 48 h before testing. The tests were performed according to EN ISO 2062:2009 using a gauge length of 250 mm and a displacement rate of 250 mm/min, on a H100KS testing equipment from Hounsfield, equipped with a 5 kN load cell. Preloads of 5 N and 7.5 N were applied to hemp and flax yarns, respectively, then the loading continued monotonically until rupture of the yarn. All the test results considered for the mechanical property calculations presented fiber rupture within the gauge length defined. The statistical study was done according to ASTM E178-16a to exclude outlying measurements [20]. The physical properties needed to calculate the yarn's cross section area (in terms of linear density and density) were reported in a previous work [21], see also Section 2.1. The yarn cross-section was considered for all cases as that obtained for the washed yarns, regarding the yarn itself as the main structural component in the system. Thus, the cross-section of the hemp and flax yarns were estimated to be 0.586 ± 0.055 mm^2 and 0.971 ± 0.08 mm^2, respectively. The Young's modulus was calculated as the tangential modulus. In a parallel investigation from the authors, hemp and flax yarns were subjected to a heat treatment similar to the conditions of the curing of the coated yarns (at 80° for three hours).

The other characterizations and tests are detailed in the supplementary materials.

3. Results

3.1. SEM analysis

SEM analysis was conducted aiming at investigating the surface morphology of the fibers and coatings, the uniformity of nanoplatelet dispersion in the polymeric phase and the quality of the interfaces at both fibril-to-polymer and GNPs-to-polymer levels. SEM results are presented in Fig. 2 and Fig. 3 noting that Fig. 2d), Fig. 3b), Fig. 3d) and Fig. 3f) are the zoomed-in micrographs of the red-squared regions of Fig. 2c), Fig. 3a), Fig. 3c) and Fig. 3e), respectively. Fig. 2a) and Fig. 2b) show the SEM micrographs of the pristine hemp fibrils collected in their longitudinal direction and the hemp fibrils-to-WPU interface acquired from a cross section of hemp-WPU/H25GNPs/0.5 % obtained by cryo-fracture, respectively. The noncoated yarns demonstrated a clean and smooth surface after washing with the sequence of ethanol/ acetone/ hexane. Fig. 2b) depicts a good WPU/fibril interfacial adhesion where the fibrils were well wet by WPU. Fig. 2c) illustrates the cross-section of the composite film formed by WPU and 0.5 wt% H25GNPs, showing homogeneity of the nanoplatelets distribution in the polymeric matrix. Good wetting of H25GNPs with the polymer as well as good interfaces are observed, see Fig. 2d). The rare clustering of the H25GNPs observed in WPU/H25GNPs/0.5 % demonstrates the effectiveness of the designed protocol and homogenous nanoparticles distribution in the polymeric matrix. Upon increasing the loading of H25GNPs to 1 % and 2 %, an increase in nanoplatelets clustering was observed, caused by the presence of a larger concentration of nanoplatelets that facilitates their interaction through Van der Waals forces and their hydrophobic nature [15 22], see Fig. 3a) and Fig. 3c). Therefore, this in turn reduced the quality of the interfacial areas as displayed by Fig. 3b) and Fig. 3d). Finally, a good dispersion homogeneity was delivered upon the PDA functionalization of H25GNPs (no clustering formation) as observed in Fig. 3e. There was an improved interfacial adhesion (less voids) between PDA/GNPs and WPU, Fig. 3f), if compared to the interface of the pristine GNPs-to-WPU, Fig. 2d).

In a good agreement with the literature, PDA conveyed a robust tool to tailor the surfaces of the materials with specific functionalities from carbon nanotubes [23 24] to graphene [25 26] and graphene oxide with WPU [18]. The performance of any nanocomposite, mainly the mechanical performance, depends at the first place on the good dispersion of the nano reinforcements within the polymeric phase, as well as the quality of the interface that allows the stress transfer from the polymer to the reinforcing nanoparticles [27].

3.2. Tensile properties

The tensile tests were carried out on coated and as-received hemp and flax yarns. The mechanical properties calculated for the tested yarns were the ultimate tensile strength (f_t), the ultimate elastic modulus (E_T) and the ultimate strain (ε_u), presented in Table 2 and Table 2S for hemp and flax, respectively. Hemp and flax yarns presented a remarkable enhancement in the mechanical properties after application of the different coating formulations mentioned in Table 2 and Table 2S. By coating hemp and flax yarns with the neat WPU, the tensile strength increased by 95 % and 20 %, respectively; the elastic modulus also increased drastically by 213 % and 88 %, respectively. This improvement of the mechanical properties of the fiber yarns may be attributed to the excellent wetting of the fiber bundles that form the yarns by the WPU/GNPs suspensions. The hydrophilic groups of WPU strongly interact with cellulose and during the crosslinking phase covalent reaction with the cellulose fibers' surface hydroxyl groups may take place. Thus, the coating acts as an adhesive holding the filament bundles together and confining the space used by the filament bundles. This

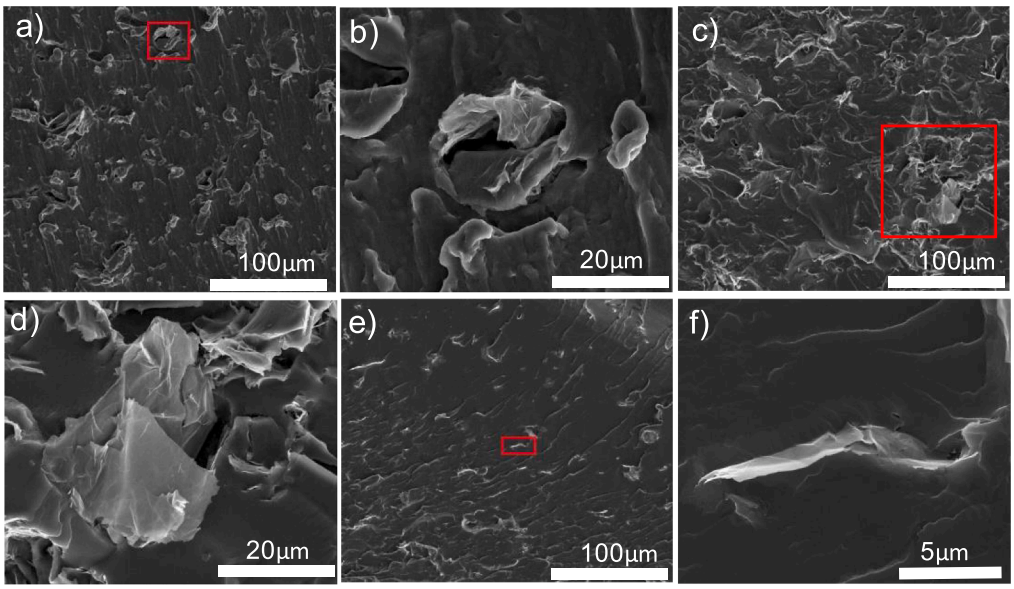

Fig. 3. SEM micrographs: a) H25GNPs distribution in WPU/H25GNPs/1%,), b) H25GNPs-to-WPU interface in WPU/H25GNPs/1%, c) H25GNPs distribution in WPU/H25GNPs/2%, d) H25GNPs-to-WPU interface in WPU/H25GNPs/2%. e) PDA/H25GNPs distribution in WPU/PDA/H25GNPs/0.5%, f) PDA/H25GNPs-to-WPU interface in WPU/PDA/H25GNPs/0.5%.

Table 2
Hemp mechanical properties.

Fibers	GNPs type and percentage (%)	f_t (MPa)*	E_T (GPa)*	ε_u (mm/mm)*
As received	0 %	220 ± 32	8 ± 1	0.0261 ± 0.002
Hemp 80° C	0 %	241 ± 40	8 ± 1	0.031 ± 0.003
Washed	0 %	335 ± 79	12 ± 1.9	0.0273 ± 0.003
Washed, WPU	0 %	429 ± 52	25 ± 4.7	0.0177 ± 0.004
Washed, WPU, no PEG/GL	H25, 0.5 %	462 ± 82	18 ± 1.9	0.0251 ± 0.004
	H25, 1 %	469 ± 51	23 ± 6	0.0218 ± 0.006
	H25, 2 %	383 ± 20	17 ± 5.1	0.0244 ± 0.007
Washed, WPU + PEG/GL	H25, 0.5 %	486 ± 26	21 ± 2.7	0.0234 ± 0.003
	H25, 1 %	491 ± 66	20 ± 2.8	0.0246 ± 0.003
	H25, 2 %	500 ± 36	17 ± 3.4	0.0305 ± 0.005
	PDA/H25, 0.5 %	534 ± 73	24 ± 5.2	0.0232 ± 0.004
	C, 0.5 %	432 ± 52	22 ± 3	0.02 ± 0.004

* The results are presented with the corresponding standard deviation.

results in an overall enhancement of the interfacial mechanical interlocking and frictional stress-transfer between the bundles. Consequently, more filaments bear the applied stress, enabling a more effective use of the yarns' mechanical properties. The ultimate strain experienced a drop of 33 % for hemp and 35 % for flax yarns if compared to the as-received ones. This drop can be related to the embrittlement induced by the neat WPU coating itself or its curing temperature.

The effect of the curing temperature on the yarns mechanical properties was separately investigated by subjecting hemp and flax yarns to a temperature similar to that of WPU curing conditions, see Fig. 4a) and Fig. 4b).

It is possible to observe two different groups: the as-received present higher initial modulus and appear to be more brittle (lower deformation at break). After heat treatment the initial modulus is lower and the stress, compared at the same strain level, is also lower; however there seems to be a plasticizing effect of the heat treatment that awards the yarns higher deformability, thus presenting higher strain at break, and thus also a little higher tensile strength, compared to the as-received yarns.

It was observed that hemp yarns coated with nanocomposites prepared with the addition of PEG and GL outperformed the yarns prepared with WPU only (see Table 2), while for flax yarns the exclusion of PEG and GL from the nanocomposites resulted in a slight increase in their tensile properties (see Table 2S). However, during tensile testing, the samples coated with nanocomposites prepared without PEG/GL exhibited a frequent rupture close to the clamping system, thus, the nanocomposites prepared without PEG/GL were excluded from further characterization. It was also observed that as the content in H25GNPs increased the tensile properties tended to decrease, principally Young's modulus, see Table 2 and Table 2S. This observation may be associated with the lower dispersion efficiency observed for higher nanoparticle contents. At higher graphene nanoplatelet contents agglomeration is expected, the nanoparticle agglomerates stabilized via Van der Waals interaction, thus creating voids in the polymer with a consequent drop in the mechanical properties. It was verified that the reinforcing effect of CGNPs was lower than H25GNPs, as the WPU/CGNPs/0.5 % composite presented similar tensile properties as WPU alone. Therefore, considering the tensile properties, the optimal coating formulation selected for further studies was based on 0.5 wt% of H25GNPs (against 1 wt% and 2 wt% GNPs: PU).

Fig. 5 illustrates the typical tensile behavior of natural cellulosic yarns (full line) and the expected tensile response of the same yarns after coating with a protecting/reinforcing polymer (dashed line). It is held that the complex yarn architecture, constituted by multiple filaments containing crystalline fibrils oriented with a tilt angle relative to the fiber axis, as well as the poor filament-to-filament bonding, induce a variable stiffness response, depicted by the full line. This tensile response features a global inelastic behavior that may be represented by two stages, first stage characterized with a lower modulus, $\acute{E}_{T,\ initial}$, corresponding to the initial yarn structure alignment along the tensile test direction, and a second stage representing the maximum stiffness of the overall yarn, $\acute{E}_T$ [28 29], which is achieved upon the diminishing of

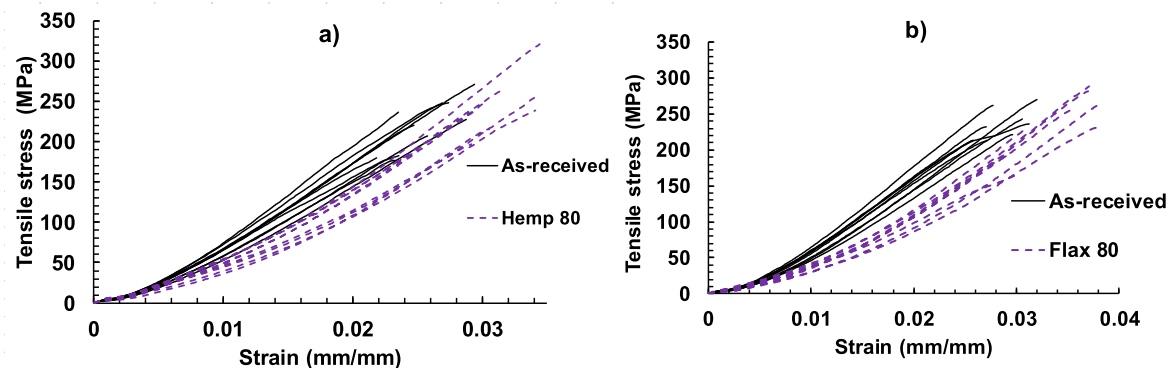

Fig. 4. Tensile properties of a) hemp and b) flax yarns before and after heat treatment at 80° C.

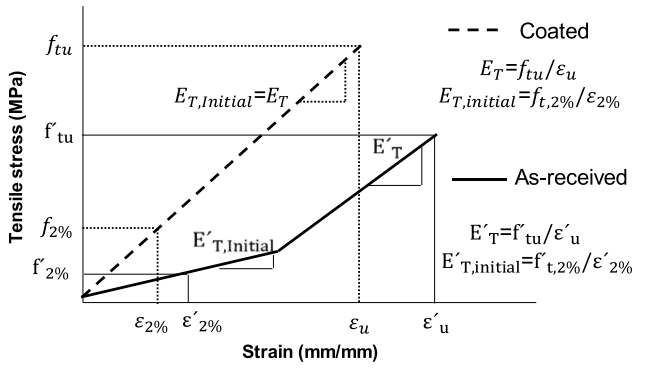

Fig. 5. Representation of typical stress–strain curves of natural fiber yarns before and after coating.

the tilt angle as well as the fibrils rearrangement in the load direction. After alignment of the fibrils, higher $\acute{E}_T$ is reached and possibly maintained until the yarn rupture [30]. However, the low $\acute{E}_{T,\ initial}$ may extend up to a considerable stress state of the yarn (up to 10–15 % of the fiber tensile strength, f_{tu}). This limits the application of natural cellulosic yarns as reinforcements for brittle matrices such as lime mortar, presenting an $\acute{E}_{T,\ initial}$ considerably lower than the mortar Young's modulus. Thus, the noncoated cellulosic yarns are inadequate for the design of NTRM systems, leading to premature cracking of the matrix before the yarns start their reinforcing effect. However, coating the yarns with a pre-designed mechanical coating can enhance the initial stiffness where it can be unified during the tensile loading, (bringing $E_T \approx E_{T,\ initial}$). The unified stiffness of the yarn may allow the required composite response and avoid premature cracking of the mortar. The ideal coating should also be designed to improve the adhesion and mechanical interlocking between the yarns and the mortar, as they exhibit weak bond behavior at yarn-to-matrix interfaces.

To illustrate, in the complex structure of natural fibers, it is possible

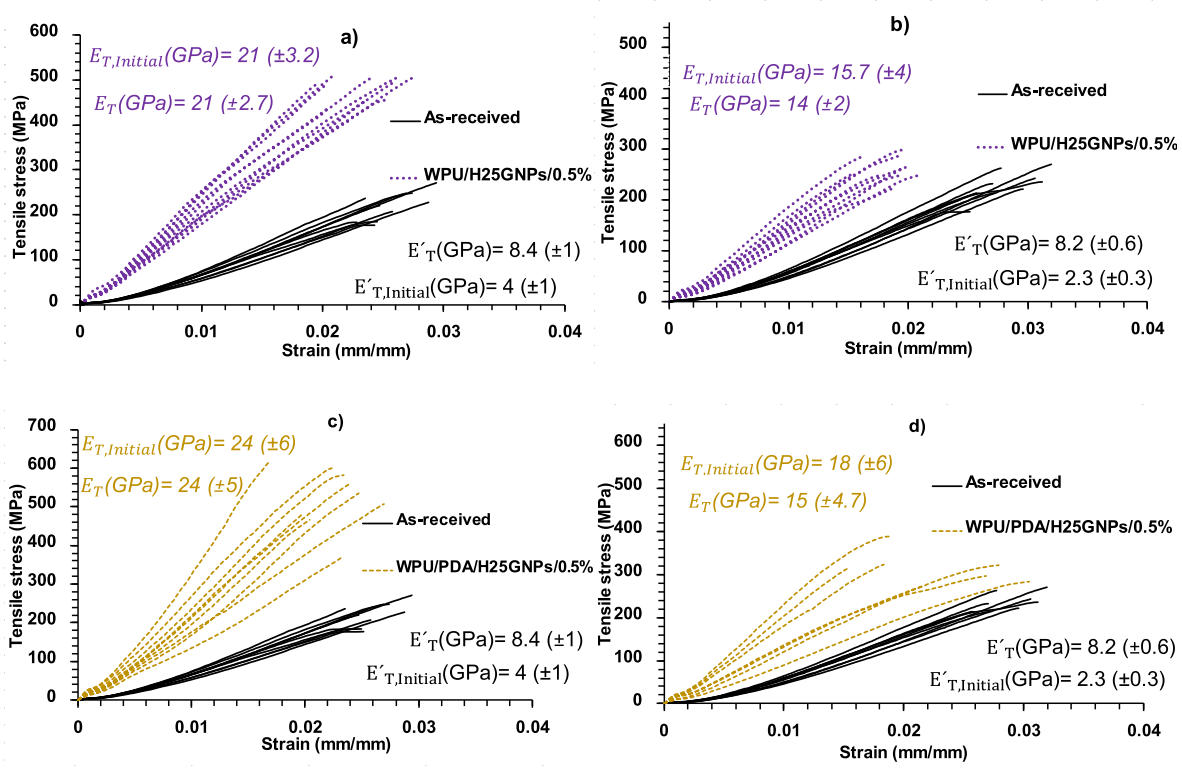

Fig. 6. Stress–strain curves before and after coating with WPU/H25GNPs/0.5% and WPU/PDA/H25GNPs/0.5% of hemp (a, c) and flax (b, d).

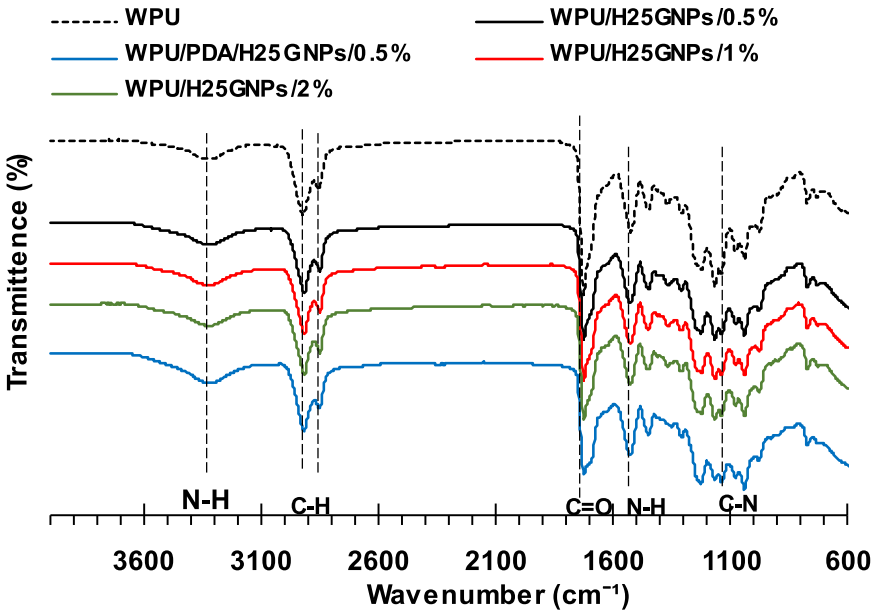

Fig. 7. ATR-FTIR spectra of WPU films reinforced with 0.5%, 1% and 2% of H25GNPs as well as 0.5% of PDA/H25GNPs.

to observe two groups of filaments, the inner filaments (core filaments) and the outer filaments [31 32]. Upon NTRM casting, the core filaments are not reached by the mortar materials, thus only the outer filaments are anchored in the mortar and are responsible for the bond behavior. This means that the non-coated yarn does not use its full capacity as a reinforcement. Therefore, after coating the yarns, a strong reinforcing system is applied to the yarn through the nanocomposites by which the stresses are evenly distributed around the yarn perimeter, yeilding it a rigid composite behavior [33]. see Fig. 1S.

Fig. 6a) depicts the stress–strain curves of WPU/H25GNPs/0.5 %-coated hemp yarns, showing an increase of 120 % and 163 % in tensile strength (f_{tu}) and elastic modulus (E_T) compared to the as-received yarns. The tensile properties of WPU/H25GNPs/0.5 %-coated flax yarns (Fig. 6b) presented a more modest increase in f_{tu} and E_T of 12 % and 75 %, respectively, relative to the as-received yarns. The functionalized WPU/PDA/H25GNPs/0.5 % coated yarns presented a remarkable improvement of the tensile properties of hemp and flax yarns, see Fig. 6c) and Fig. 6d). Compared to hemp-WPU/H25GNPs/0.5 %, a further increase of 10 % and 15 % for f_{tu} and E_T, respectively, was observed, which may be attributed to chemical bonding between PDA/H25GNPs and the WPU. Finally, the initial stiffness ($E_{T,\ initial}$) of the coated yarns, calculated at 2 % of f_{tu}, and its corresponding strain $\varepsilon_{2\%}$, demonstrated the same trend as E_T, calculated at f_{tu}, see Fig. 6. For instance, WPU/H25GNPs-0.5 %-coated hemp and flax yarns demonstrated a significantly higher initial stiffness $E_{T,\ initial}$ if compared to their as-received counterparts (425 % and 580 %, respectively). The WPU/H25GNPs/0.5 % coating (with/without functionalization of GNPs) recovered the low initial stiffness of bast natural fibers, and this is essential to guarantee a reproducible design of NTRM.

3.3. Infrared spectroscopy

Attenuated Total Reflectance–Fourier Transform Infrared Spectroscopy analysis (ATR-FTIR) was conducted to investigate the chemistry of the nanocomposites in terms of functional groups and their possible reactivity. Fig. 7 presents the ATR-FTIR spectra of the nanocomposite films collected in the waveumber range 600–4000 cm^{-1}. As it was expected, the FTIR spectra could not provide a very robust tool to detect the various chemical changes in the nanocomposite cast with different ratios (0.5 %, 1 % and 2 %). The spectra of reinforced WPU maintained the significant bands of the neat WPU in both the functional group and fingerprint regions, indicating that the bulk polymeric phase was not damaged by the protocol formulation nor upon oxidation. The peaks observed near 3323 cm^{-1}, 2918 cm^{-1} and 2852 cm^{-1} correspond to N—H, C—H asymetric and symetric stretching, respectively, in polyurethane [34].

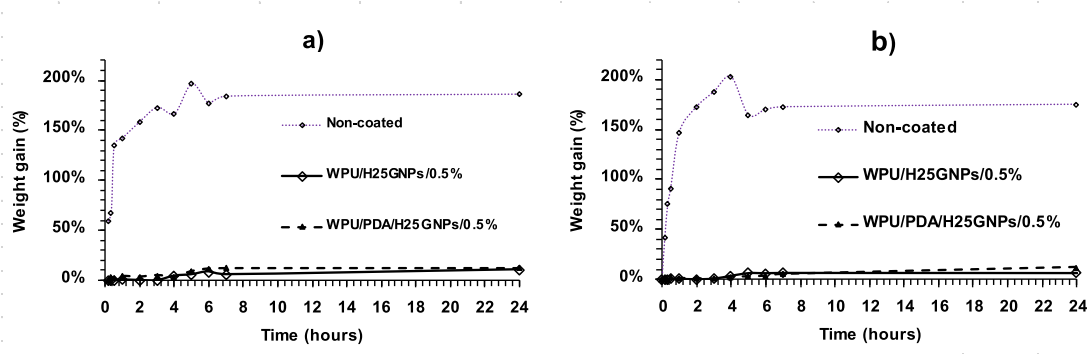

Fig. 8. Water absorption trend of a) hemp and b) flax.

All the nanocomposites demostrated a sharp band around 1729 cm^{-1} corresponding to carbonyl group stretching deformation (C═O) present in urethane [35]. PDA present in WPU/PDA/H25GNPs/0.5 % is a multi-species polymer and it is rich with catehcolic hydroxyl groups and different monomers of amino groups, Fig. 3S [36]. The amines present in the PDA as nucleophiles tend to attack positively charged carbons such as the carbonyl groups present in the polyurethane and, thus, form imine (C═N) via Schiff base reaction and/ or an amide (C-N) via Michael reaction. The vibration of N—H is denoted by the band near 1530 cm^{-1} [37]. The medium band observed near 1137 cm^{-1} is related to C—N stretching [37], and it can be due to reaction between the PDA and WPU. It was possible to see that this peak promoted a slightly higher intensity in case of WPU/PDA/H25GNPs/0.5 % than the other nanocomposite scenarios and it can be assigned to amines in the PDA [38 39].

3.4. Water absorption test

This test was conducted to assess the enhancement in water uptake resistance conveyed by the designed nanocomposite-based coating when the coated yarns are placed under water. This analysis is important since natural fibers are hydrophilic, and the mortar matrix retains water and hydration salts, weakening the cellulosic material of the natural fiber. The results of water absorption tests for hemp and flax yarns before and after applying the optimal coatings (containing 0.5 wt% of H25GNPs with or without functionalization) are presented in Fig. 8a) and Fig. 8b), respectively. The hydrophilicity of as-received hemp and flax yarns is reflected on the weight gain of 60 % and 40 %, respectively, observed after 10 min of immersion. After 3 h, the water absorption reached a plateau indicating saturation of these yarns, with a maximum weight increase of 185 % and 175 % for hemp and flax yarns, respectively. This high-water uptake may be ascribed to the exposure of the hydrophilic cellulose, enhanced by the washing protocol used to partially extract lignin and other components, as reported in a previous work [21]. Conversely, both hemp and flax yarns coated with WPU/H25GNPs/0.5 % and WPU/PDA/H25GNPs/0.5 % significantly reduced the water uptake. The non-coated yarns reached their saturation point after 3 h immersion, while the coated yarns showed almost 0 % weight gain after that period. The saturation level of the coated hemp and flax was approximately 10 % weight, and was reached above 6 h of immersion and maintained still until 24 h. Although neat WPU is not strongly hydrophobic, the addition of the 2D high-aspect ratio GNPs will decrease the permeability to water due to their hydrophobicity and 2D morphology that induce a barrier effect [15]. Additionally, the nanocomposite coating may provide a restraining barrier to the fibers' swelling, limiting the access and space for the accommodation of water molecules within the hydrophilic parts in fiber lumen [10].

3.5. Raman spectroscopy

Raman spectroscopy is a powerful tool to characterize graphitic materials [40]. This technique was used to confirm the functionalization of the GNPs and to monitor their dispersion in the WPU matrix. Such characteristics are related to the mechanical properties of the nanocomposites. The Raman spectrum of a graphitic material is informative about the stacking of the carbon sp^2 graphene planes, the presence of sp^3 carbon due to chemical reactions and bonding of other chemical functions, and other relevant structural aspects [41]. Here, Raman spectroscopy was used to study changes in GNPs structure due to defects or increase of sp^3 carbon upon functionalization, as well as to detect the reinforcing GNPs in the WPU matrix [42]. The typical Raman spectrum of GNPs shows the characteristic bands: G (~1580 cm^{-1}), D (~1350 cm^{-1}), D' (1610 ~ 1620 cm^{-1}) and G' (or 2D, ~ 2700 cm^{-1}) [40 43]. The G mode is present in all carbon-based materials with conjugated C═C double bonds, reflecting the in-plane bond stretching motion of pairs of sp^2 carbon atoms [40 42]. The D mode is a breathing mode that is forbidden in perfect graphene, becoming active in the presence of

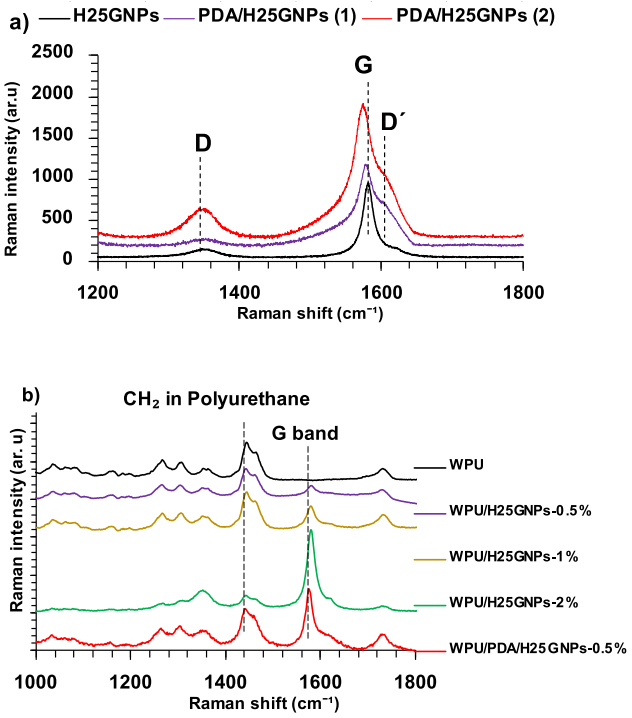

Fig. 9. Raman spectra of the nanoparticles and their films.

disorders. It indicates a disturbance of the hexagonal sp^2 carbon network by chemical bonding such as that observed on a graphene edge or a structural defect [44 45]. The D' band shows as a shoulder peak of the G band and it is due to the formation of sp^3 carbon [42 46 45]. The G' (or 2D) band is a second-order mode that is not related to graphene defects, always presenting high intensity in graphene. The shape and position of the G' band varies with the number of graphene layers [46]. Fig. 9a) presents the Raman spectra of as-received H25GNPs and two samples of PDA functionalized H25GNPs, showing the G, D, D' bands. The pristine GNPs present a low intensity D band, indicating a dominant sp^2 carbon structure, while both of PDA/H25GNPs samples show an intensity increase mainly due to chemical reaction that transform part of the sp^2 carbon to sp^3 hybridization, see the deconvoluted spectra in Fig. 4S. The presence of PDA at the GNPs surface is also confirmed by the broadening of the G band and presence of the D' band for PDA/H25GNPs, as compared to the pristine GNPs, see Fig. 9a). Moreover, in accordance with Bin Fei et al [24] PDA itself shows a broad Raman peak around 1580 cm^{-1}, contributing to the broadening of the G band. The overall analysis of the Raman spectra underlined the successful functionalization of H25GNPs via Mussel-inspired surface modification [47].

The Raman spectra of the WPU composite films were collected and normalized for the peak corresponding to CH_2 bending in WPU, see Fig. 9b). The pristine WPU film presented a typical spectrum of polyurethane with a predominant peak ~ 1440 cm^{-1} characteristic of (CH_2) bending [48]. The Raman spectrum of WPU/H25GNPs in Fig. 9b) shows the presence of the G band of the GNPs, increasing its intensity as the weight load of GNPs increases (i.e., from 0.5 % to 2 %). WPU/PDA/H25GNPs/0.5 % also presents the characteristic G band at ~ 1579 cm^{-1}, Fig. 9b), with higher intensity than that observed in WPU/H25GNPs/0.5 %. This increase in intensity may be indicative of good PDA/GNPs dispersion and enhanced interface of PDA/GNPs with the WPU matrix, thus exposing a larger GNPs covered area exposed to the Raman analysis.

3.6. Thermogravimetric analysis

TGA analysis was carried out to monitor the water adsorption of the

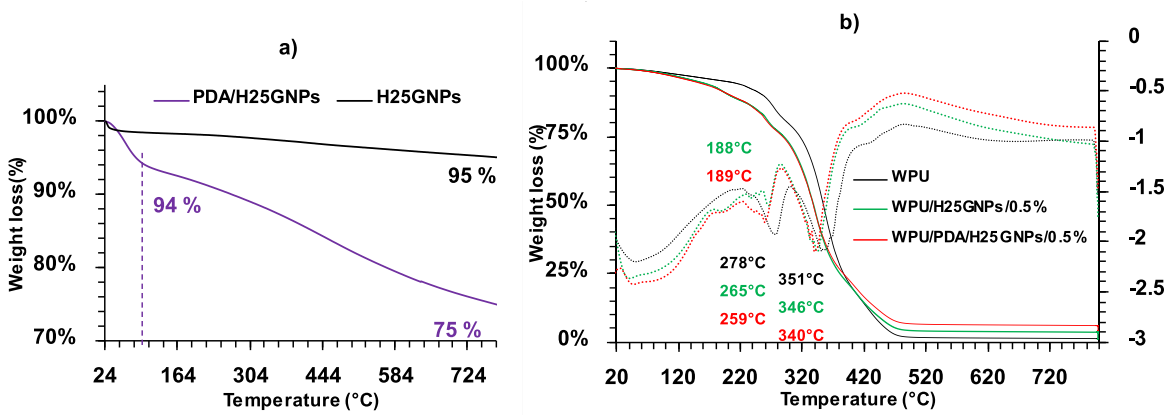

Fig. 10. TGA analysis of a) H25GNPs/PDA/H25GNPs and b) WPU, WPU/H25GNPs/0.5% and WPU/PDA/H25GNPs/0.5%, where the dotted lines represent the derivative of the TGA curves.

functionalized GNPs as well as their functionalization degree in terms of weight fraction. The TGA results of the GNPs and corresponding WPU composite films are presented in Fig. 10. The pristine H25GNPs showed a stable thermal response along time up to 800 °C under inert atmosphere, with a maximum of 5 % weight loss observed at the end of the analysis. This weight loss is due to the thermal decomposition of the oxygen-containing groups present in low concentration in the as-received GNPs. Conversely, the PDA/H25GNPs exhibited a weight loss throughout the heating process to reach a 75 % residual weight at 800 °C. In the latter case the initial 6 % weight loss at 100 °C is attributed to water present in the sample, thus an estimate of the PDA/H25GNPs weight functionalization level indicates ~ 19 % wt. The thermal degradation trend delivered by the nanoparticles before and after functionalization is in agreement with references [15 24 18]. TGA was also used to evaluate the thermal stability of the coatings for the desired application in inorganic matrices. The WPU films demonstrated a typical response of the thermal degradation of polyurethanes. Similarly to the results highlighted in the references [35 17], two dominant stages are normally assigned to the degradation of pristine WPU, at 278 °C and 351 °C, as depicted in Fig. 10b), and they are linked to the decomposition of the hard segment and the soft segment of WPU, respectively. The WPU nanocomposites also showed the two-stage degradation with a shift to lower temperatures. The small weight loss observed at ~ 190 °C in both WPU/H25GNPs/0.5 % and WPU/PDA/H25GNPs/0.5 % is associated to the vaporization of the lower molecular weight components of the nanocomposite, PEG and GL. TGA results confirm that the coating is thermally stable within the temperature range required for the desired application.

4. Conclusion

This work presents a novel application of graphene nanoplatelets/waterborne polyurethane to enhance the mechanical properties and the durability of natural fibers, aiming to make them suitable for NTRM casting. The authors presented a step-by-step description of the scientific aspects and preparation protocols, using environmentally friendly procedures, to deliver the product (i.e., nanocomposite-impregnated hemp yarns) at laboratory scale. The optimal formulation was selected from composites prepared with 0.5, 1 and 2 wt% of GNPs dispersed in WPU, and was found to be 0.5 wt%, based the tensile properties. The surface functionalization of H25GNPs was tailored using a Mussel-inspired chemical method that further enhanced the dispersion of the functionalized graphene (PDA/H25GNPs) in the aqueous polymer suspension and provided good interfacial bonding with the polymer. Both WPU/H25GNPs/0.5 % and WPU/PDA/H25GNPs/0.5 % demonstrated to be excellent coating materials to enhance the water resistance of hemp and flax fibers. The coated yarns delivered the mechanical response required for a functional NTRM system, presenting an increase of the initial modulus, relative to the uncoated yarns, of 425 % for hemp and 580 % for flax yarns. Thus, the coated yarns provide a promising solution for developing smart NTRM systems with different functionalities in the future. Further investigation will focus on the composite natural fibers interfacial bond with mortar materials as well as the up-scaling process and cost analysis for the optimized textile reinforcement design.

CRediT authorship contribution statement

Ali Abbass: Conceptualization, Methodology, Investigation, Data curation, Writing - original draft. **Maria C. Paiva:** Conceptualization, Methodology, Supervision, Writing - review & editing. **Daniel V. Oliveira:** Conceptualization, Methodology, Supervision, Funding acquisition. **Paulo B. Lourenço:** Supervision, Funding acquisition, Writing - review & editing. **Raul Fangueiro:** Resources, Writing - review & editing.

Declaration of Competing Interest

The authors declare the following financial interests/personal relationships which may be considered as potential competing interests: Paulo B. Lourenco reports financial support was provided by Foundation for Science and Technology. Ali Abbass, Maria C. Paiva, Daniel V. Oliveira, and Paulo B. Lourenço have patent #PT 118295 pending to INPI.

Data availability

The authors are unable or have chosen not to specify which data has been used.

Acknowledgments

This work was partially financed by FEDER funds through the Competitively Factors Operational Program (COMPETE) and by national funds through the Foundation for Science and Technology (FCT) within the scope of the project POCI-01-0145-FEDER-007633. IPC acknowledges the support of FCT through National Funds References UIDB/05256/2020 and UIDP/05256/2020. The authors wish to acknowledge the Portuguese foundation for science and technology (FCT) for the PhD scholarship granted to the first author (SFRH/BD/144106/2019).

Appendix A. Supplementary data

Supplementary data to this article can be found online at https://doi.org/10.1016/j.compositesa.2022.107379.

References

[1] Valluzzi MR, da Porto F, Garbin E, Panizza M. Out-of-plane behaviour of infill masonry panels strengthened with composite materials. Mater Struct 2014;47(12):2131–45.

[2] de Felice G, De Santis S, Garmendia L, Ghiassi B, Larrinaga P, Lourenço PB, et al. Mortar-based systems for externally bonded strengthening of masonry. Mater Struct Constr 2014;47(12):2021–37.

[3] Dalalbashi A, Ghiassi B, Oliveira DV, Freitas A. Fiber-to-mortar bond behavior in TRM composites : ffect of embedded length and fiber configuration. Compos Part B 2018;152(March):43–57. https://doi.org/10.1016/j.compositesb.2018.06.014.

[4] Candamano S, Crea F, Coppola L, De Luca P, Coffetti D. Influence of acrylic latex and pre-treated hemp fibers on cement based mortar properties. Constr Build Mater 2021;273:121720. https://doi.org/10.1016/j.conbuildmat.2020.121720.

[5] Mercedes L, Bernat-maso E, Gil L. In-plane cyclic loading of masonry walls strengthened by vegetal-fabric- reinforced cementitious matrix (FRCM) composites. Eng Struct 2020;221(February):111097. https://doi.org/10.1016/j.engstruct.2020.111097.

[6] Trochoutsou N, Di M, Pilakoutas K, Guadagnini M. Bond of Flax Textile-Reinforced Mortars to Masonry. Constr Build Mater 2021;284:122849. https://doi.org/10.1016/j.conbuildmat.2021.122849.

[7] Wei J, Meyer C. Degradation rate of natural fiber in cement composites exposed to various accelerated aging environment conditions. Corros Sci 2014;88:118–32. https://doi.org/10.1016/j.corsci.2014.07.029.

[8] Mercedes L, Gil L, Bernat-maso E. Mechanical performance of vegetal fabric reinforced cementitious matrix (FRCM) composites. Constr Build Mater 2018;175:161–73. https://doi.org/10.1016/j.conbuildmat.2018.04.171.

[9] Glenn Veigas M, Najimi M, Shafei B. Case Studies in Construction Materials Cementitious composites made with natural fibers : Investigation of uncoated and coated sisal fibers. Case Stud Constr Mater 2022;16(September):e00788. https://doi.org/10.1016/j.cscm.2021.e00788.

[10] Rocha Ferreira S, De Andrade Silva F, Lima PRL, Dias Toledo Filho R. Effect of fiber treatments on the sisal fiber properties and fiber-matrix bond in cement based systems. Constr Build Mater 2015;101:730–40. https://doi.org/10.1016/j.conbuildmat.2015.10.120.

[11] Ferrara G, Pepe M, Martinelli E, Dias Tolêdo Filho R. Influence of an impregnation treatment on the morphology and mechanical behaviour of flax yarns embedded in hydraulic lime mortar. Fibers 2019;7:30. https://doi.org/10.3390/fib7040030.

[12] Rocha Ferreira S, Sena Neto AR, Silva De Andrade F, de Souza Jr G, Dias Toledo Filho R. The influence of carboxylated styrene butadiene rubber coating on the mechanical performance of vegetable fibers and on their interface with a cement matrix. Constr Build Mater 2020;262:120770. https://doi.org/10.1016/j.conbuildmat.2020.120770.

[13] Choi SH, Kim DH, Raghu AV, Reddy KR, Lee H-I, Yoon KS, et al. Properties of graphene/waterborne polyurethane nanocomposites cast from colloidal dispersion mixtures. J Macromol Sci Part B Phys 2012;51(1):197–207.

[14] Król P, Król B, Zenker M, Subocz J. Composites prepared from the waterborne polyurethane cationomers-modified graphene. Part II. Electrical properties of the polyurethane films. Colloid Polym Sci 2015;293(10):2941–7. https://doi.org/10.1007/s00396-015-3697-2.

[15] Cunha E, Paiva MC. Composite Films of Waterborne Polyurethane and Few-Layer Graphene — Enhancing Barrier, Mechanical, and Electrical Properties. Compos Sci 2019:9–11. https://doi.org/10.3390/jcs3020035.

[16] Cuinat-guerraz N, Dumont M, Hubert P. Environmental resistance of flax / bio-based epoxy and flax / polyurethane composites manufactured by resin transfer moulding. Compos Part A 2016;88:140–7. https://doi.org/10.1016/j.compositesa.2016.05.018.

[17] Han Y, Jiang Y, Hu J. Collagen incorporation into waterborne polyurethane improves breathability, mechanical property, and self-healing ability. Compos Part A 2020;133(November):105854. https://doi.org/10.1016/j.compositesa.2020.105854.

[18] Zhang S, Zhang D, Li Z, et al. Polydopamine functional reduced graphene oxide for enhanced mechanical and electrical properties of waterborne polyurethane nanocomposites. J Coat Technol Res 2018;15:1333–41. https://doi.org/10.1007/s11998-018-0082-3.

[19] Feng J, Fan H, Zha DA, Wang L, Jin Z. Characterizations of the formation of polydopamine-coated halloysite nanotubes in various pH environments. Langmuir 2016;32(40):10377–86. https://doi.org/10.1021/acs.langmuir.6b02948.

[20] American National Standard, Dealing With Outlying Observations, E 178 – 02. In Annual Book of ASTM Standards, 2002.

[21] Abbass A, Paiva MC, Oliveira DV, Lourenço PB, Fangueiro R. Insight into the Effects of Solvent Treatment of Natural Fibers Prior to Structural Composite Casting : Chemical, Physical and Mechanical Evaluation. Fibers 2021;9(54):1–18. https://doi.org/10.3390/fib9090054.

[22] Cunha E, Duarte F, Proença MF, Paiva MC. Few-layer graphene aqueous suspensions for polyurethane composite coatings. MRS Adv 2017;2(1):57–62. https://doi.org/10.1557/adv.2016.640.

[23] Wang H, Wang E, Liu Z, Gao D, Yuan R, Sun L, et al. A novel carbon nanotubes reinforced superhydrophobic and superoleophilic polyurethane sponge for selective oil-water separation through a chemical fabrication. J Mater Chem A 2015;3(1):266–73.

[24] Fei B, Qian B, Yang Z, Wang R, Liu WC, Mak CL, et al. Coating carbon nanotubes by spontaneous oxidative polymerization of dopamine. Carbon N Y 2008;46(13):1795–7.

[25] Chen K, Tian Q, Tian C, Yan G, Cao F, Liang S, et al. Mechanical Reinforcement in Thermoplastic Polyurethane Nanocomposite Incorporated with Polydopamine Functionalized Graphene Nanoplatelet. Ind Eng Chem Res 2017;56(41):11827–38.

[26] Zhu P, Weng L, Zhang X, Wang X, Guan L, Liu L. Graphene@poly(dopamine)-Ag core–shell nanoplatelets as fillers to enhance the dielectric performance of polymer composites. J Mater Sci 2020;55(18):7665–79. https://doi.org/10.1007/s10853-020-04557-y.

[27] Yang L, Phua SL, Toh CL, Zhang L, Ling H, Chang M, et al. Polydopamine-coated graphene as multifunctional nanofillers in polyurethane. RSC Adv 2013;3(18):6377.

[28] Trochoutsou N, Di M, Pilakoutas K, Guadagnini M. Mechanical Characterisation of Flax and Jute Textile-Reinforced Mortars. Constr Build Mater 2021;271:121564. https://doi.org/10.1016/j.conbuildmat.2020.121564.

[29] Shah DU, Schubel PJ, Licence P, et al. Hydroxyethylcellulose surface treatment of natural fibres: the new 'twist' in yarn preparation and optimization for composites applicability. J Mater Sci 2012;47:2700–11. https://doi.org/10.1007/s10853-011-6096-1.

[30] Baley C. Analysis of the flax fibres tensile behaviour and analysis of the tensile stiffness increase. Compos Part A, 2002;33(7):939–48. https://doi.org/10.1016/S1359-835X(02)00040-4.

[31] Homoro O, Michel M, Baranger TN. Pull-out response of glass yarn from ettringite matrix: Effect of pre-impregnation and embedded length. Compos Sci Technol 2019;170:174–82.

[32] Slama AC, Gallias JL, Fiorio B. Study of the pull-out test of multifilament yarns embedded in cementitious matrix. J Compos Mater 2021;55(2):169–85. https://doi.org/10.1177/0021998320946368.

[33] Reinhardt HSH-W, Krüger M, Bentur A, Brameshuber W, Banholzer B, Manfred Curbach, Jesse F, Mobasher B, Peled A. Textile Reinforced Concrete - State-of-the-Art Report of RILEM TC 201-TRC. In State-of-the-Art Report of RILEM Technical Committee 201-TRC: Textile Reinforced Concrete, RILEM Publications SARL, 2006, pp. 83–131.

[34] Molina GA, Elizalde-Mata A, Hernández-Martínez ÁR, Fonseca G, Cruz Soto M, Rodríguez-Morales ÁL, et al. Synthesis and Characterization of Inulin-Based Responsive Polyurethanes for Breast Cancer Applications. Polymer (Guildf) 2020;12(4). https://doi.org/10.3390/polym12040865.

[35] Tian K, Su Z, Wang H, Tian X, Huang W, Xiao C. N-doped reduced graphene oxide / waterborne polyurethane composites prepared by in situ chemical reduction of graphene oxide. Compos Part A 2017;94:41–9. https://doi.org/10.1016/j.compositesa.2016.11.020.

[36] Liebscher J. Chemistry of Polydopamine – Scope, Variation, and Limitation. Eur J Org Chem 2019;2019(31-32):4976–94.

[37] Asefnejad A, Khorasani MT, Behnamghader A, Farsadzadeh B, Bonakdar S. Manufacturing of biodegradable polyurethane scaffolds based on polycaprolactone using a phase separation method : physical properties and in vitro assay. Int J Nanomedicine 2011;6:2375–84. https://doi.org/10.2147/IJN.S15586.

[38] Ha Y-M, Kim YN, Jung YC. Rapid and Local Self-Healing Ability of Polyurethane Nanocomposites Using Photothermal Polydopamine-Coated Graphene Oxide Triggered by Near-Infrared Laser. Polymers (Basel) 2021;13(1274). https://doi.org/10.3390/polym13081274.

[39] Wang S, Zhu J, Rao Y, Li B, Zhao S, Bai H, et al. Polydopamine Modified Graphene Oxide-TiO 2 Nanofiller for Reinforcing Physical Properties and Anticorrosion Performance of Waterborne Epoxy Coatings. Appl Sci 2019;9(18):3760.

[40] Pimenta MA, Dresselhaus G, Dresselhaus MS, Cançado LG, Jorio A, Saito R. Studying disorder in graphite-based systems by Raman spectroscopy. Phys Chem Chem Phys 2007;9(11):1276–90.

[41] Dresselhaus MS, Jorio A, Hofmann M, Dresselhaus G, Saito R. Perspectives on Carbon Nanotubes and Graphene Raman Spectroscopy. Nano Lett 2010;10:751–8. https://doi.org/10.1021/nl904286r.

[42] Pereira P, Ferreira DP, Araújo JC, Ferreira A, Fangueiro R. The Potential of Graphene Nanoplatelets in the Development of Smart and Multifunctional Ecocomposites. Polymer 2020;12(10):2189.

[43] Malard LM, Pimenta MA, Dresselhaus G, Dresselhaus MS. Raman spectroscopy in graphene. Phys Rep 2009;473(5–6):51–87. https://doi.org/10.1016/j.physrep.2009.02.003.

[44] Niyogi S, Bekyarova E, Itkis ME, Zhang H, Shepperd K, Hicks J, et al. Spectroscopy of covalently functionalized graphene. Nano Lett 2010;10(10):4061–6.

[45] Gao G, Liu D, Tang S, Huang C, He M, Guo Yu, et al. Heat-Initiated Chemical Functionalization of Graphene. Sci Rep 2016;6(1). https://doi.org/10.1038/srep20034.

[46] Young RJ, Kinloch IA, Gong L, Novoselov KS. The mechanics of graphene nanocomposites : A review. Compos Sci Technol 2012;72(12):1459–76. https://doi.org/10.1016/j.compscitech.2012.05.005.

[47] Kanyong P, Krampa FD, Aniweh Y, Awandare GA. Polydopamine-functionalized graphene nanoplatelet smart conducting electrode for bio-sensing applications. Arab J Chem 2020;13(1):1669–77. https://doi.org/10.1016/j.arabjc.2018.01.001.

[48] Romanova V, Begishev V, Karmanov V, Kondyurin A, Maitz MF. Fourier transform Raman and Fourier transform infrared spectra of cross- linked polyurethaneurea films synthesised from solutions. J Raman Spectrosc 2002;33(October):769–77.